Supplementary Tables

Table S1. Primers used for amplifying gene fragments or plasmid construction

Genes/Plasmids	Primer Sequence (5′→3′)	Amplicon sizes (bp)	Enzyme site
Hh	Forward: GAATTTAGCCGTTAATAGGGAG Reverse: GCGAGTAATCCGTCCGTTGA	454	*Bsr*G I
Kif3a	Forward: GTGACAAGAAGGAGCGTGACT Reverse: TCTTACCATTGTATCCCTCCAG	273	*Age* I
Foxj1 TALEN1	Forward 1: GCCACCACTCCAAACCAAAGG Reverse 1: GCAGATCAGGGTTGCGTAGGA	505	*Aji* I
Foxj1 TALEN2	Forward 2: GCCACCACTCCAAACCAAAGG Reverse 2: CTGCCAGCTGGGTTCGGCCA	610	*Bsi*W I
Hh-pXT7	Forward: AATTCGAATTTAGCCGTTAATAGGGAG		*Eco*R I
	Reverse: CTAGTACACACAGCCGAGTAGACACTT		*Spe* I
Smo-pXT7	Forward: GGTACCTTTCCACCATGTTGAGGAGCG		*Kpn* I
	Reverse: CTAGTGGTTCTTCACAGTACTCTGTATC		*Spe* I
Hh-myc-pXT7	Forward1: TTGGCAGATCGGTACCGAATTCATGGCGGGGGT ACTAGCGCG Reverse1: TGAATCCGTCGCCGTTGGGTGT Forward2: ACCCAACGGCGACGGATTCAAAAGAGCTAGCTA CCATGGAGC Reverse2: GATCCTAGTCAGTCACTAGTCTACTCAAGAGGCC TTGAGTTC		
caSmo-myc-pXT7	Forward: ATACGTATGTCACTTATCATAAAGAGCTAGCTAC CATGGAGC Reverse: GATCCTAGTCAGTCACTAGTCTACTCAAGAGGCC TTGAGTTC		

Supplementary Figures

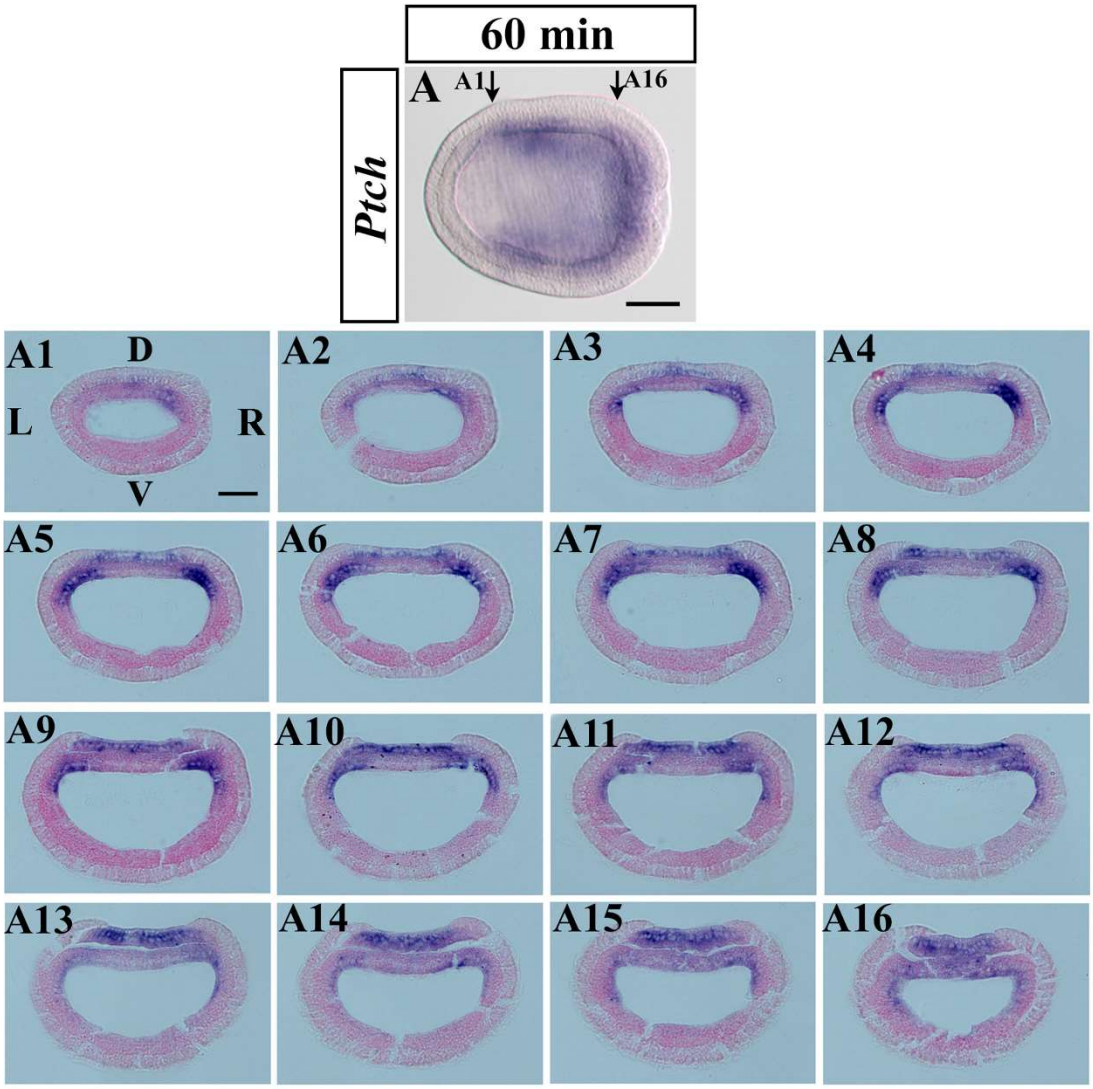

Figure S1. Asymmetric *Ptch* expression in the paraxial mesoderm of amphioxus embryo. (A) The expression of *Ptch* in WT embryo at stage 60 minutes after G5, showing weak asymmetric signal in the anterior paraxial mesoderm when observed from the dorsal side. (A1-A16) Serial transverse sections of the embryo in panel A, between the two arrows. Scale bar in A or A1 is 50 μm.

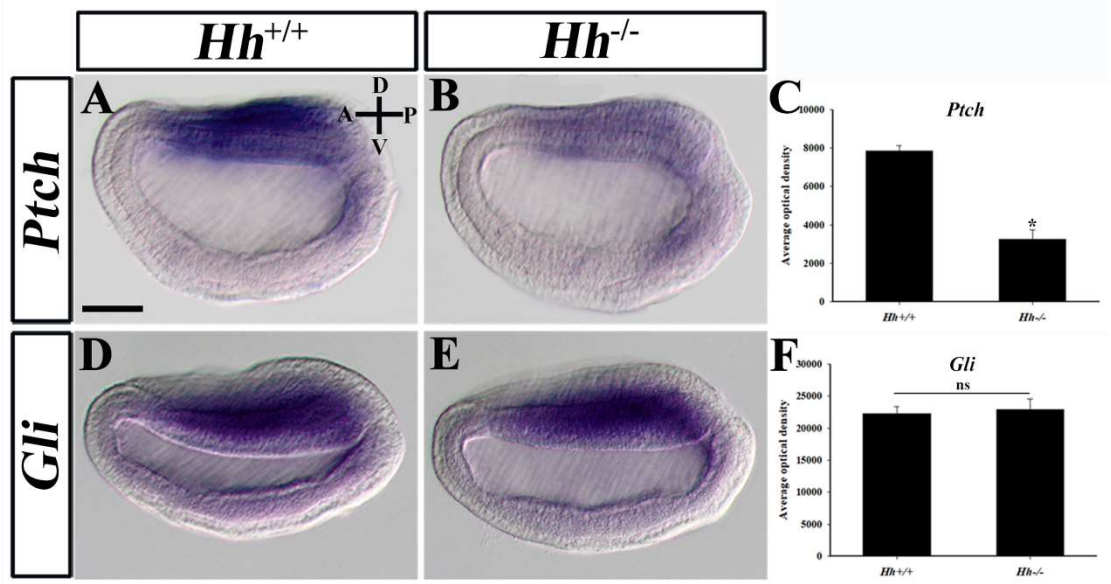

Figure S2. The expression of *Ptch* and *Gli* in *Hh* knockout embryos. (A-C) The expression of *Ptch* was decreased in *Hh* knockout embryos ($P<0.05$, n=4). Scale bar is 50 μm. (D-F) The expression of *Gli* was not significantly different between WT ($Hh^{+/+}$) and *Hh* knockout embryos ($P>0.05$, n=4). * represents statistical significance, ns: not significant.

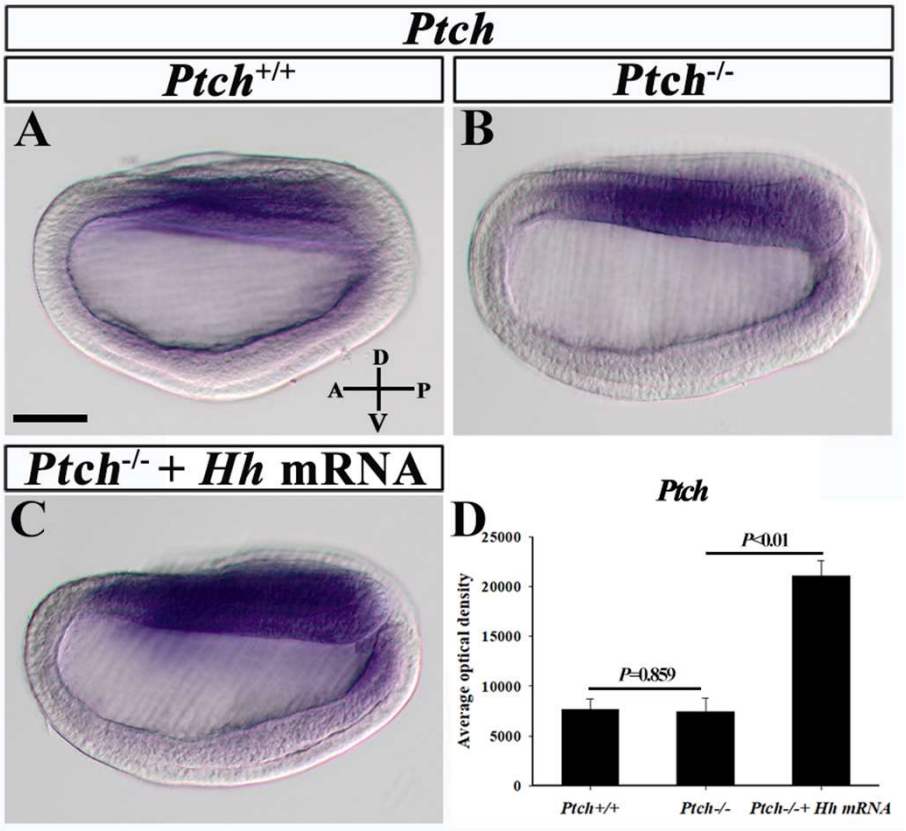

Figure S3. The expression of *Ptch* does not increase in *Ptch* knockout embryos. (A and B) The expression of *Ptch* in WT or *Ptch* knockout embryos. (C) The expression of *Ptch* was increased in *Ptch* knockout embryos injected with *Hh* mRNA. Left-lateral view with anterior to the left. The scale bar in A is 50 μm, and applies to B and C. (D) The optical density of *Ptch* expression in WT, *Ptch* knockout embryos and *Ptch* knockout embryos injected with *Hh* mRNA. The expression of *Ptch* was not significantly different between WT and *Ptch* knockout embryos ($P>0.05$, n=4), but was remarkably up-regulated in *Ptch* knockout embryos injected with *Hh* mRNA ($P<0.05$, n=4).

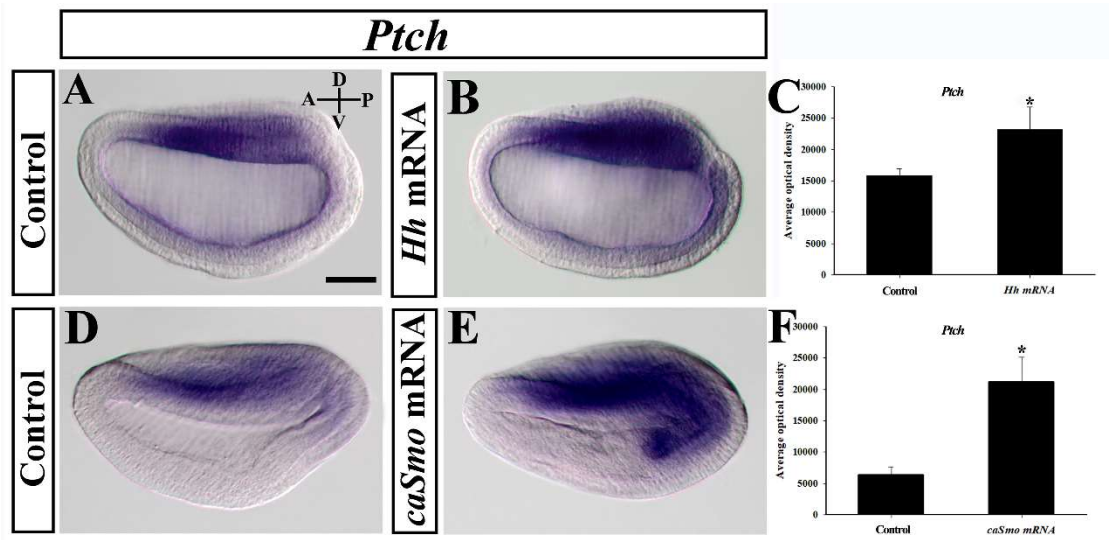

Figure S4. *Ptch* expression is increased in *Hh* or *caSmo* mRNA-injected embryos. Left-lateral view with anterior to the left. The scale bar (50 μm) in A applies to all panels. (A, B) The expression of *Ptch* in control and *Hh* mRNA-injected embryos. (C) The optical density of *Ptch* expression in control and *Hh* mRNA-injected embryos (n=6, $P<0.05$). (D, E) The expression of *Ptch* in control and *caSmo* mRNA-injected embryos. (F) The optical density of *Ptch* expression in control and *caSmo* mRNA-injected embryos (n=6, $P<0.05$). * represents statistical significance.

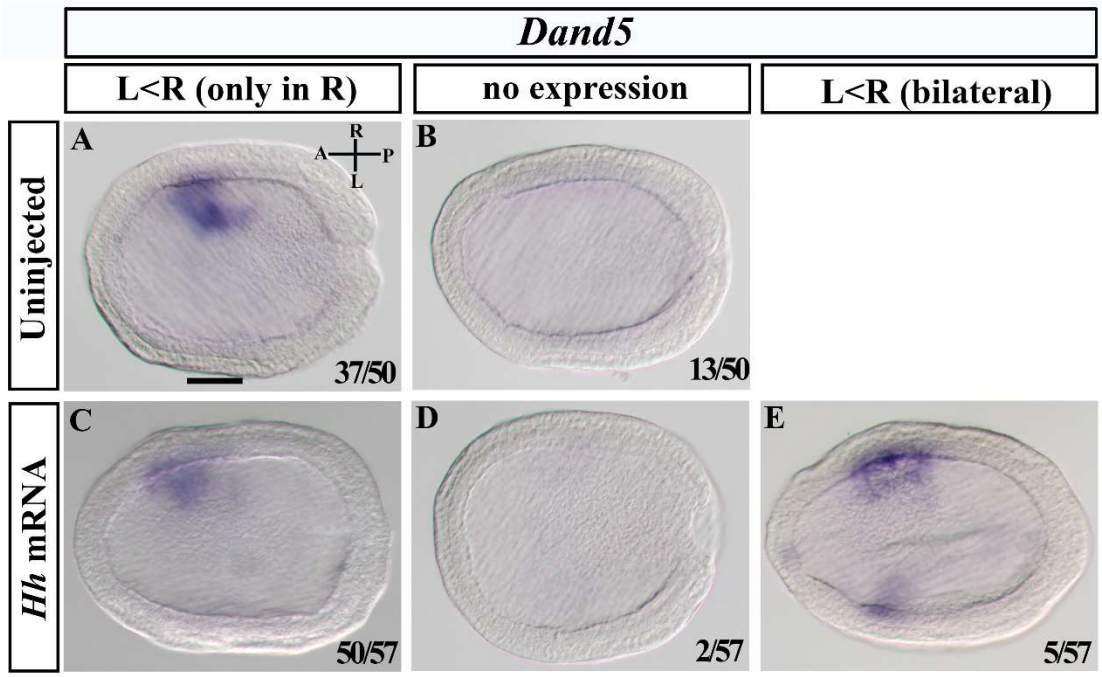

Figure S5. *Hh* mRNA injection rescues *Dand5* expression (R>L) in $Hh^{-/-}$ embryos, but could not induce L=R or L>R *Dand5* expression. Dorsal view with anterior to the left. (A, B) Expression patterns of *Dand5* in offspring of $Hh^{+/-}$ heterozygotes. (A) Right-side specific *Dand5* expression in WT/$Hh^{+/-}$ embryos. (B) Loss of *Dand5* expression in $Hh^{-/-}$ embryos. (C-E) Expression patterns of *Dand5* in *Hh* mRNA injected offspring of $Hh^{+/-}$ heterozygotes. Most of the injected embryos show right-side specific *Dand5* expression (C), and a few of them show no (D) or L<R (bilateral) *Dand5* expression (E). Numbers in the bottom right corner of a panel show the number of times the phenotype was observed in the total number of embryos examined. Scale bar (50 μm) in A applies to all panels.

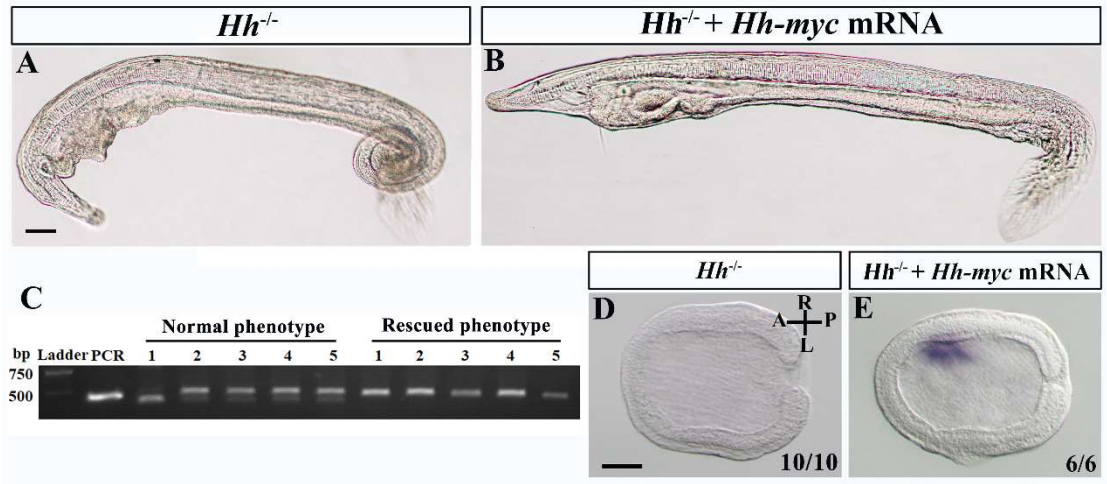

Figure S6. *Hh-myc* mRNA injection rescues the L-R morphological defects and *Dand5* expression in *Hh*$^{-/-}$ amphioxus. (A) The phenotype of *Hh*$^{-/-}$ larvae, showing a curled head, no mouth, ventralized gill slits and twisted tail. (B) Morphological restoration of *Hh*$^{-/-}$ larvae after injection of *Hh-myc* mRNA. (C) Genotyping of *Hh-myc* mRNA-injected offspring of *Hh*$^{+/-}$ heterozygotes. The normal phenotype refers to morphology of WT larvae, and the rescued phenotype refers to morphology as shown in panel B. (D) The expression of *Dand5* in *Hh*$^{-/-}$ embryos. (E) The expression of *Dand5* in *Hh*$^{-/-}$ embryos injected with *Hh-myc* mRNA. The injection rescued asymmetric *Dand5* expression in *Hh*$^{-/-}$ embryos. Scale bar in A or D represents 50 μm.

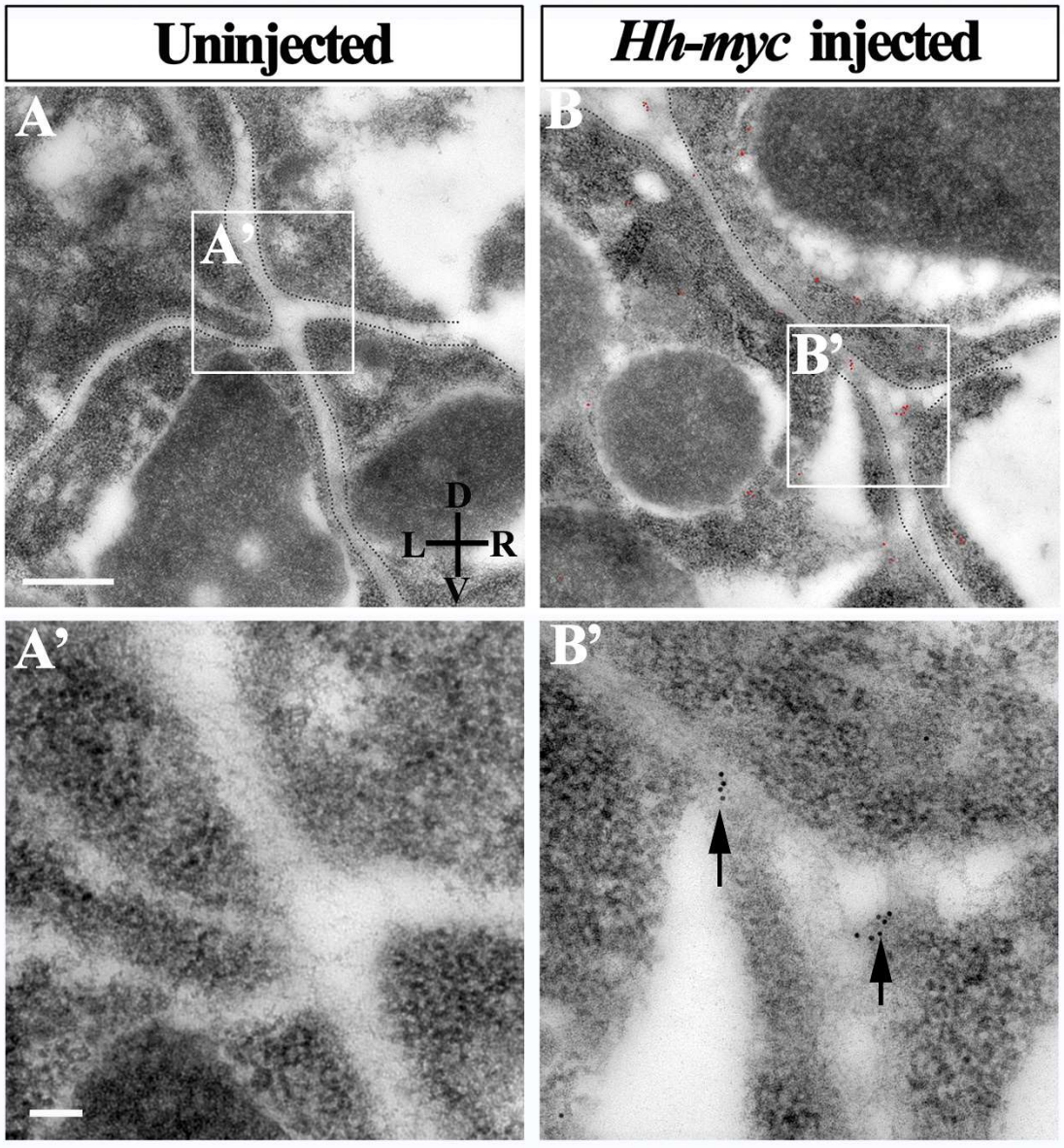

Figure S7. Immuno-EM localization of Hh-Myc fusion protein in the right side of paraxial mesoderm of *Hh-myc* mRNA-injected embryo. (A, B) Immuno-EM image of the right side of uninjected and the *Hh-myc* mRNA-injected embryos at early neurula stage. The dotted lines indicate the boundary of each cell, and the red dots represent Hh-Myc protein labelled with gold particles. R: Right; L: Left. D: Dorsal; V: Ventral. Scale bar = 500 nm. (A') Local zoom of the region in the box in panel A. Hh-Myc fusion protein is not observed in uninjected embryos. (B') Local zoom of the region in the box in panel B. Arrows point to Hh-Myc fusion protein localized to the extracellular of paraxial mesoderm. Scale bar in A' is 100 nm.

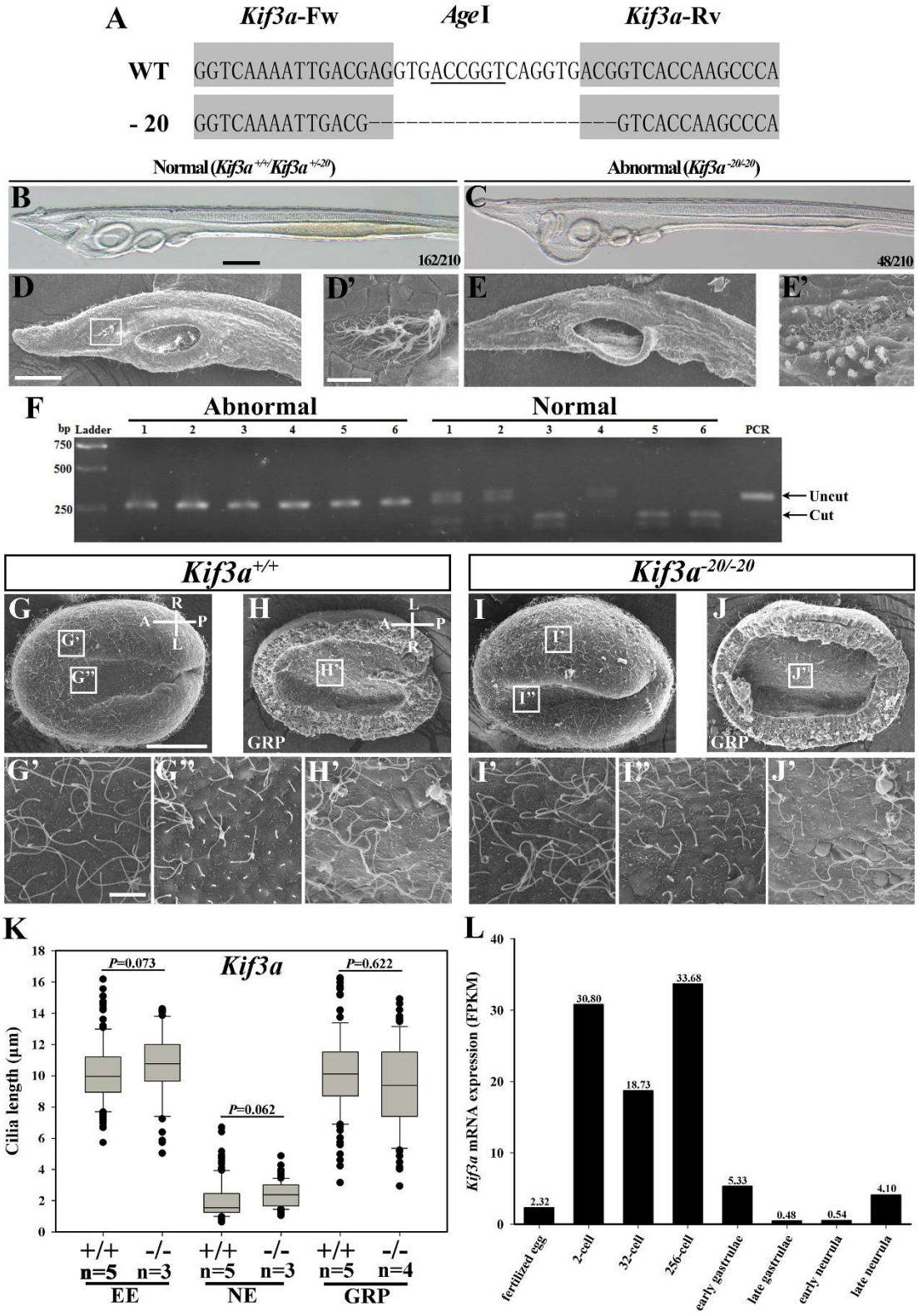

Figure S8. The ciliogenesis in *Kif3a* knockout amphioxus mutant. (A) The binding sites for *Kif3a* TALEN pairs (greyed) and the mutation type used in the study. (B and D) Left lateral view of WT/*Kif3a*$^{+/-}$ larvae. Scale bar in B or D is 50 μm. (D') Local

zoom of the preoral pit in the box in D, showing abundant cilia in this region. Scale bar in D' is 10 μm. (C and E) Left lateral view of *Kif3a*$^{-/-}$ larvae. The larva developed an enlarged mouth. (E') Local zoom of the preoral pit in the box in D, showing sparse cilia in this region. Numbers in the bottom right corner of panel B and C show the number of times the phenotype was observed in the total number of embryos examined. (F) Genotype analysis of abnormal and normal phenotype larvae using PCR assay. All six larvae of abnormal phenotype are *Kif3a*$^{-/-}$ mutants, and all six larvae of normal phenotype are WT or *Kif3a*$^{+/-}$ mutants. (G-J) SEM analysis of epithelial ectodermal (EE), neural ectodermal (NE) and gastrocoel roof plate (GRP) cilia of WT and *Kif3a*$^{-/-}$ early neurula. Anterior to the left. Scale bar (50 μm) in G applies to G-J and that (5 μm) in G' applies to G'-J'. (K) Quantification of cilia length in *Kif3a*$^{+/+}$ and *Kif3a*$^{-/-}$ embryos. The cilia length on EE, NE or GRP cells was not significant different between WT and *Kif3a*$^{-/-}$ embryos. n represents number of embryos analyzed, 20-40 cilia from each region were counted for every embryo. (L) The expression pattern of *Kif3a* during embryonic development according to transcriptome dataset.

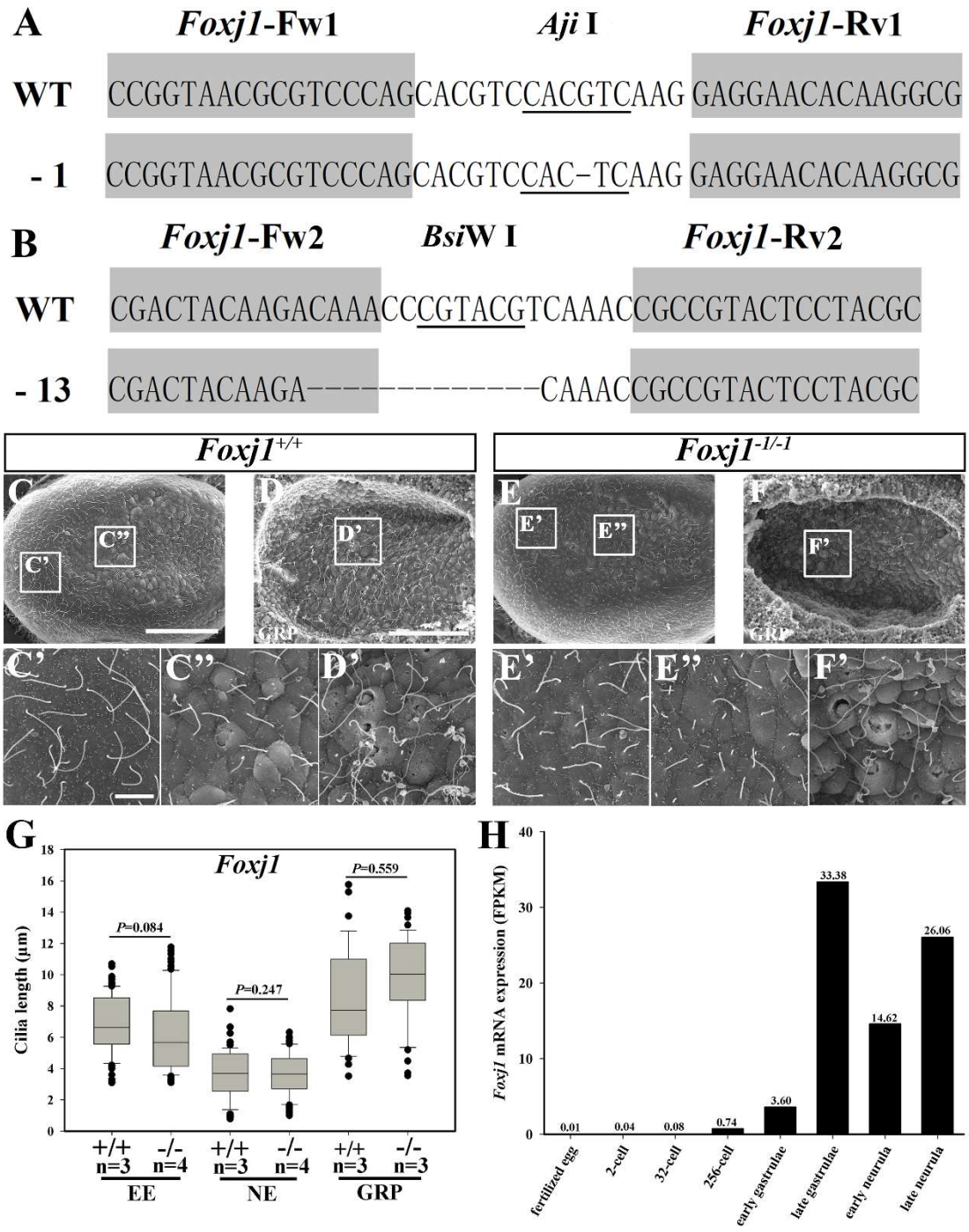

Figure S9. The ciliogenesis in *Foxj1* mutants. (A, B) The binding sites for two *FoxJ1* TALEN pairs (greyed) and the mutation types used in the study. (C-F) SEM analysis of epithelial ectodermal (EE), neural ectodermal (NE) and gastrocoel roof plate (GRP) cilia of *Foxj1*$^{+/+}$ and *Foxj1*$^{-1/-1}$ embryos. Anterior to the left. Scale bar in C or D is 50 μm. Scale bar in C' is 5 μm. (G) Quantification of cilia length in *Foxj1*$^{+/+}$ and *Foxj1*$^{-1/-1}$ embryos. The cilia length on EE, NE or GRP cells was not significant different between WT and *FoxJ*$^{-1/-1}$ embryos. n represents number of embryos analyzed, 20-40 cilia from each region were counted for every embryo. (H) The expression pattern of *Foxj1* during embryonic development according to transcriptome dataset.

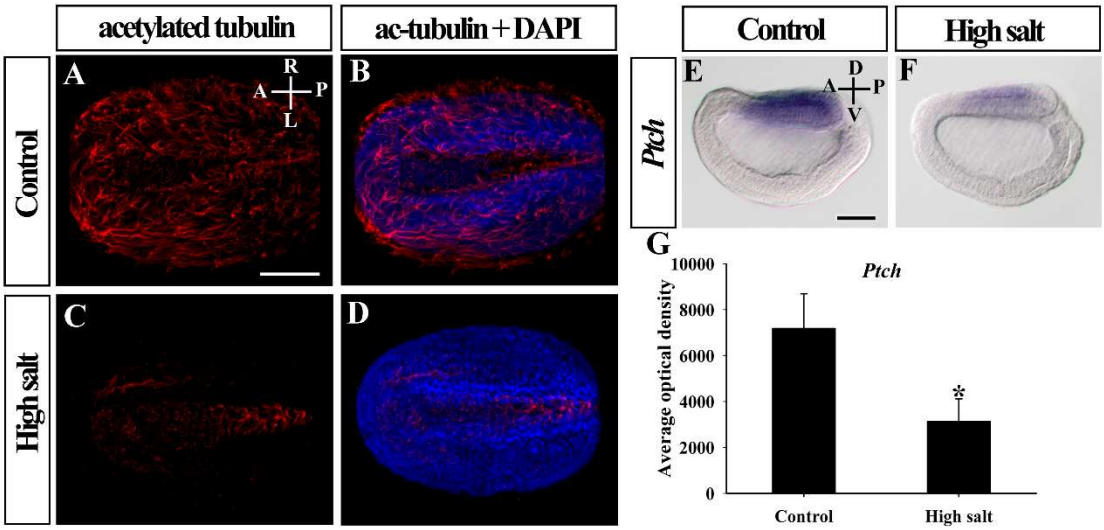

Figure S10. Removal of cilia results in down-regulation of Hh signaling activity in amphioxus. (A-D) Cilia in control and high salt (HS) treatment embryos, displaced by immunofluorescence with the cilia-specific acetylated tubulin antibody (red). Images in panels A-D were taken from the dorsal side with anterior to the left. Cell nucleuses are labelled with DAPI (blue). Most cilia in epidermal ectoderm and neurectoderm were removed by HS treatment. Scale bar is 50 μm. (E, F) The expression of *Ptch* in control and HS-treated embryos. Left lateral view with anterior to the left. Scale bar in E is 50 μm. (G) The average optical density in control and HS-treated embryos. It was significantly decreased in HS-treated embryos ($P < 0.01$, n=6). * represents statistical significance.

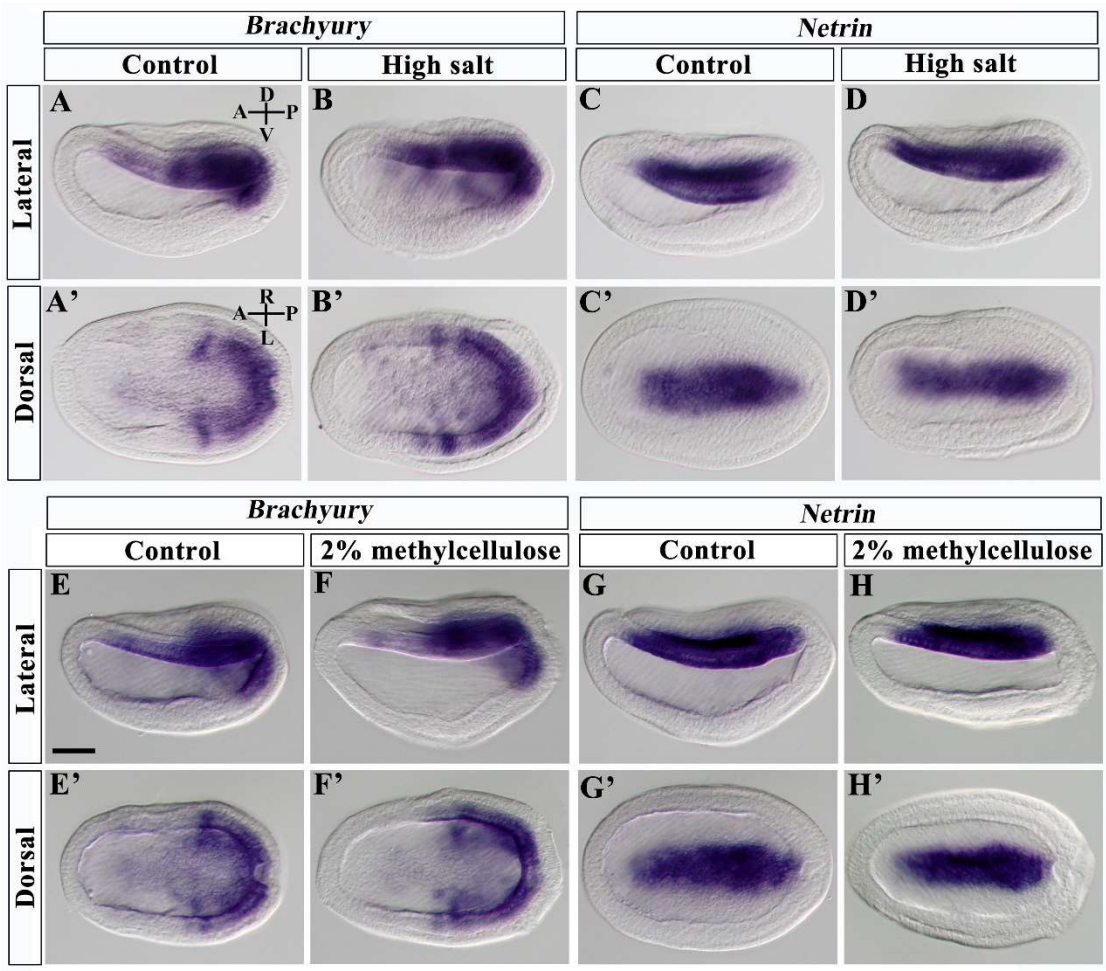

Figure S11. The expression pattern of midline structure marker genes in high salt treated and methylcellulose treated embryos at early neurula stage. (A-D) The expression of *Brachyury* and *Netrin* in control or high salt treated embryos. There was no obvious difference between control and the treated embryos. (E-H) The expression of *Brachyury* and *Netrin* in control or methylcellulose treated embryos. There was no obvious difference between control and treated embryos. The scale bar (50 μm) in E applies to all panels.

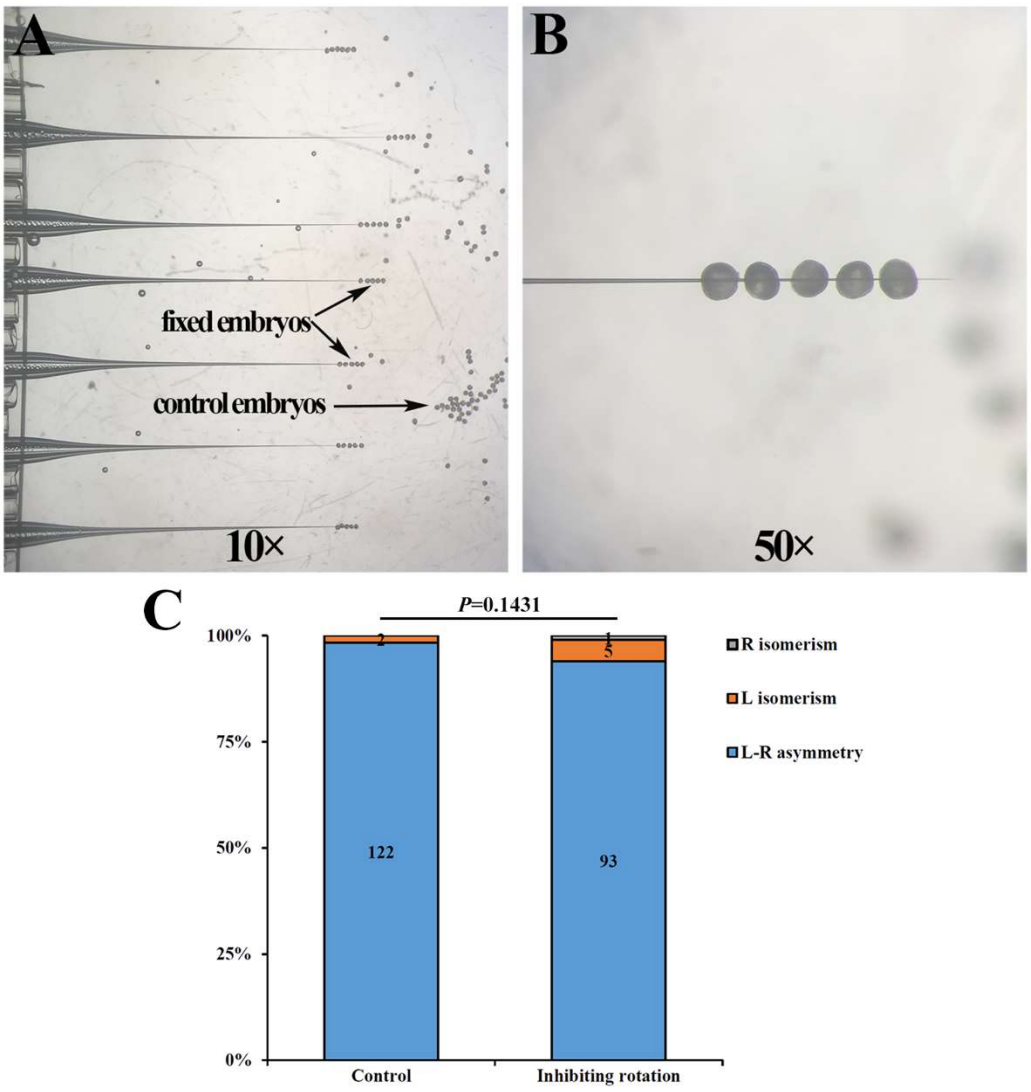

Figure S12. Embryo rotation is not essential for L-R asymmetry development in amphioxus. (A, B) 10× and 50× optical magnification of embryos, respectively. The embryos were fixed by threading them on very fine glass needles at G4 stage. (C) Percentages of embryos showing each type of phenotypes. The numbers in the column represent the number of each phenotype observed.

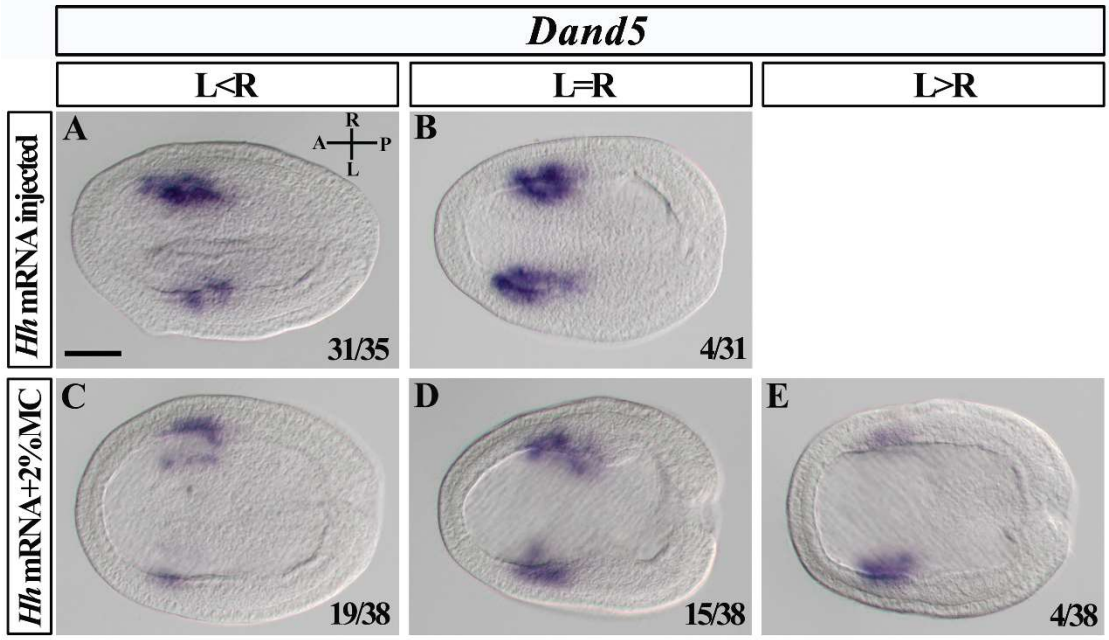

Figure S13. Inhibiting cilia movement increases the frequency of bilateral (L=R) *Dand5* expression in *Hh* mRNA injected wildtype embryos. Images in panels A-E were taken from the dorsal view with anterior to the left. (A, B) *Dand5* expression patterns in *Hh* mRNA injected embryos. (C-E) *Dand5* expression patterns in *Hh* mRNA injected embryos cultured in 2% methylcellulose. Numbers in the bottom right corner of a panel show the number of times the phenotype was observed in the total number of embryos examined. Scale bar (50 μm) in A applies to all panels.

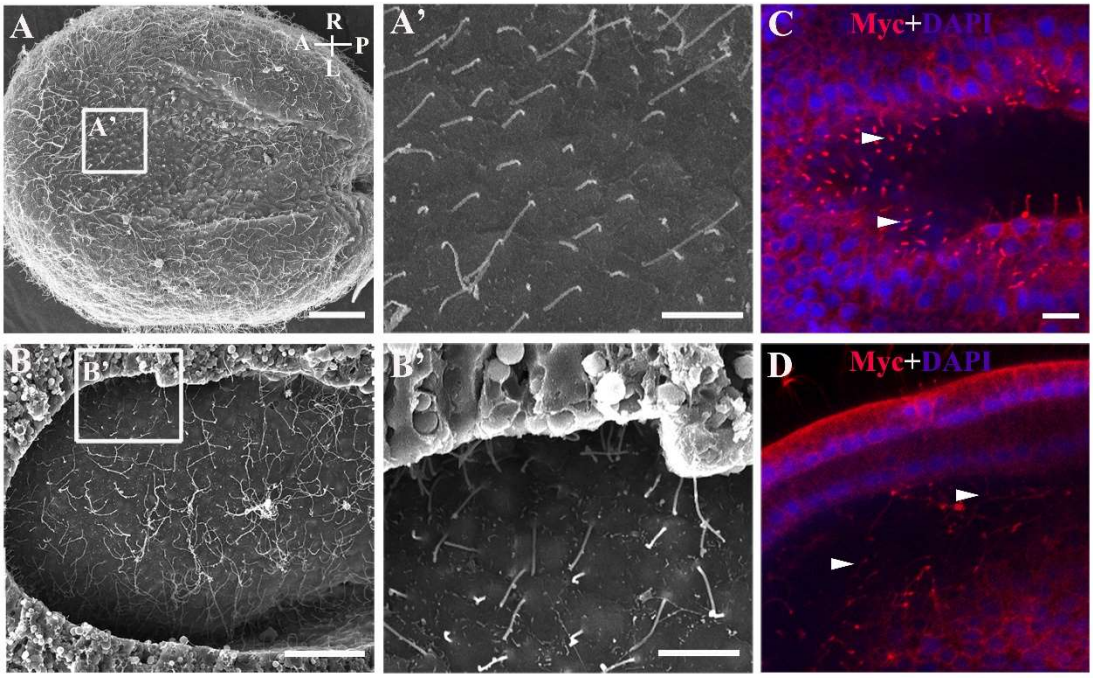

Figure S14. Hh-receiving cells own motile cilia and Smo localizes to these cilia. (A and A') SEM analysis of cilia on neural ectodermal cells of wildtype early neurula embryo. Dorsal view with anterior to the left. A' is a local zoom of the region in the box in panel A. Scale bars in A or A' is 20 or 5 μm, respectively. (B and B') SEM analysis of cilia on paraxial mesodermal cells of wildtype early neurula embryo. Ventral view with anterior to the left. B' is a local zoom of the region in the box in panel B. Scale bar in B or B' is 20 or 5 μm, respectively. (C and D) Localization of caSmo fusion protein in the cilia of neural ectodermal cells and paraxial mesodermal cells. Image C was dorsal view focusing on the neuroderm. Image D was dorsal view focusing on the paraxial mesoderm. caSmo fusion protein was labelled with the Myc antibody (red) and cell nucleuses were labelled with DAPI (blue). The arrowheads point to the cilia location of caSmo fusion protein. Scale bar in C is 10 μm.

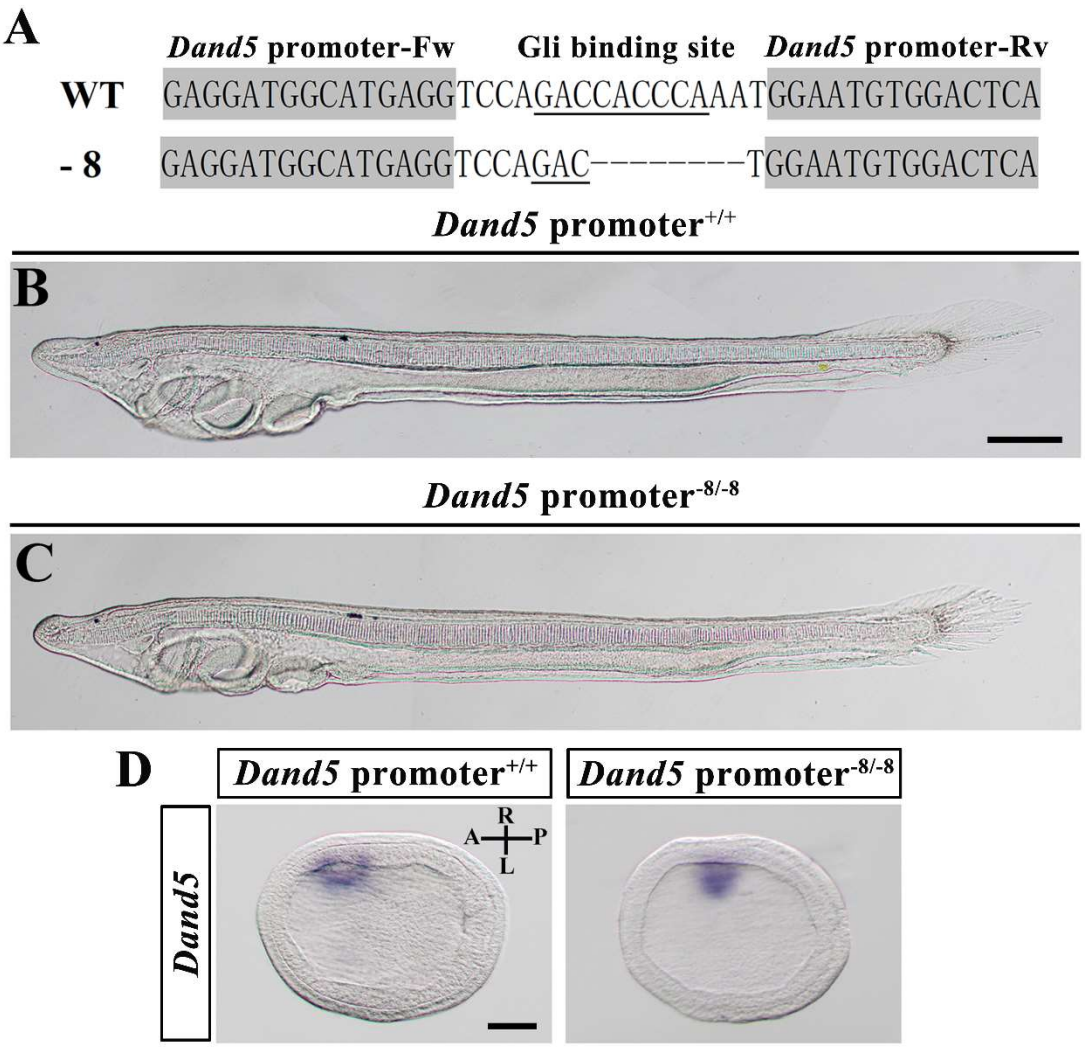

Figure S15. TALEN pairs targeting Gli binding site in *Dand5* promoter and phenotype analysis of the F2 embryos. (A) The binding site for the TALEN pair (greyed) and the mutation type used in the study. The Gli binding site in the spacer was underlined. (B and C) Left lateral view of the *Dand5* promoter$^{+/+}$ larva and *Dand5* promoter$^{-8/-8}$ larva. No obvious morphological difference was observed between them. (D) Expression patterns of *Dand5* in *Dand5* promoter$^{+/+}$ embryos and *Dand5* promoter$^{-8/-8}$ embryos. No obvious expression difference was observed between them. Image in D was taken from the dorsal view with anterior to the left. Scale bar in B or D is 50 μm.

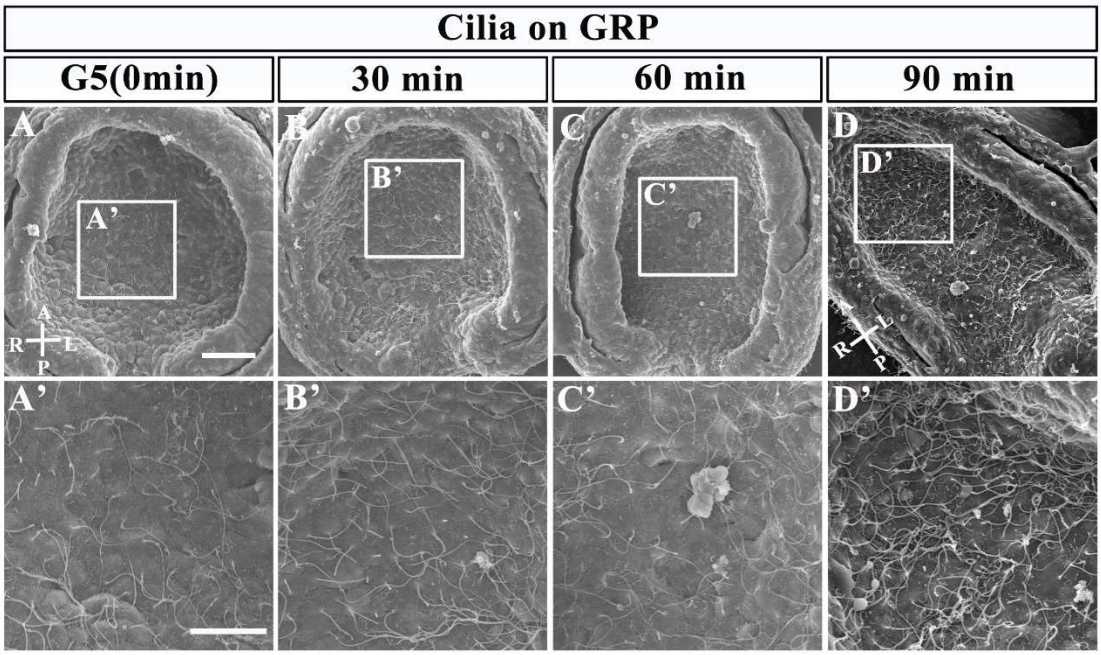

Figure S16. Observation of cilia on gastrocoel roof plate (GRP). Images in panels A-D were taken from the ventral view. 'A' anterior; 'P' posterior; 'L' left side; 'R' right side. (A-D) SEM analysis of cilia on GRP, time at G5 stage was defined as 0 minute, and 3 stages after that were adopted in the analysis. (A'-D') Local zoom of the region in the box in panel A-D, respectively. Scale bar in A or A' is 20 or 10 μm, respectively.

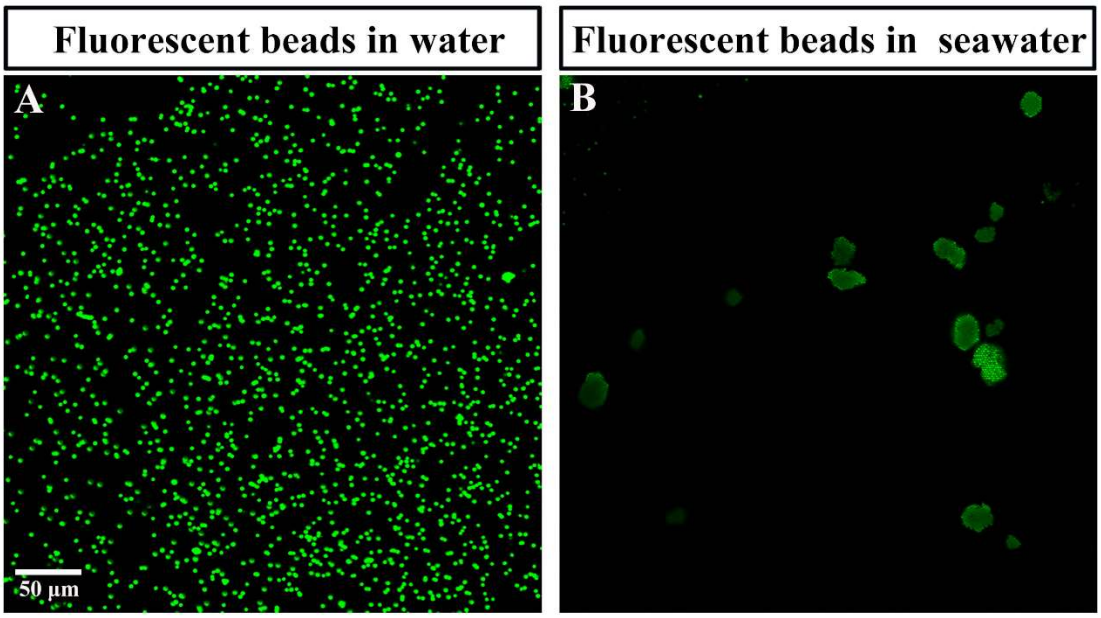

Figure S17. Dispersion of fluorescent beads in water and seawater. (A) Fluorescent beads were well dispersed in water. (B) Fluorescent beads easily gathered into big blocks in seawater.

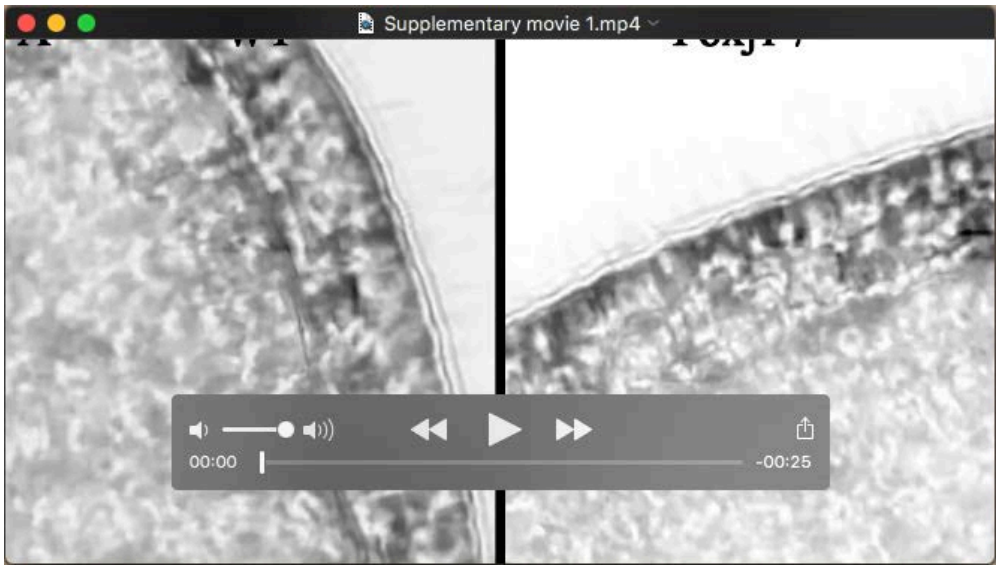

Movie 1. Cilia movement of *Foxj1*$^{-1/-1}$ homozygous mutants are of no apparent defects. Real-time movie of *Foxj1*$^{-1/-1}$ neurula embryo reveals normal cilia movement on the epithelial ectodermal cells, neural ectodermal cells and gastrocoel roof plate cells, compared to that in wildtype embryos. A, B or C in the movie showed ciliary motility in epithelial ectoderm, neural ectoderm or gastrocoel roof plate, respectively.

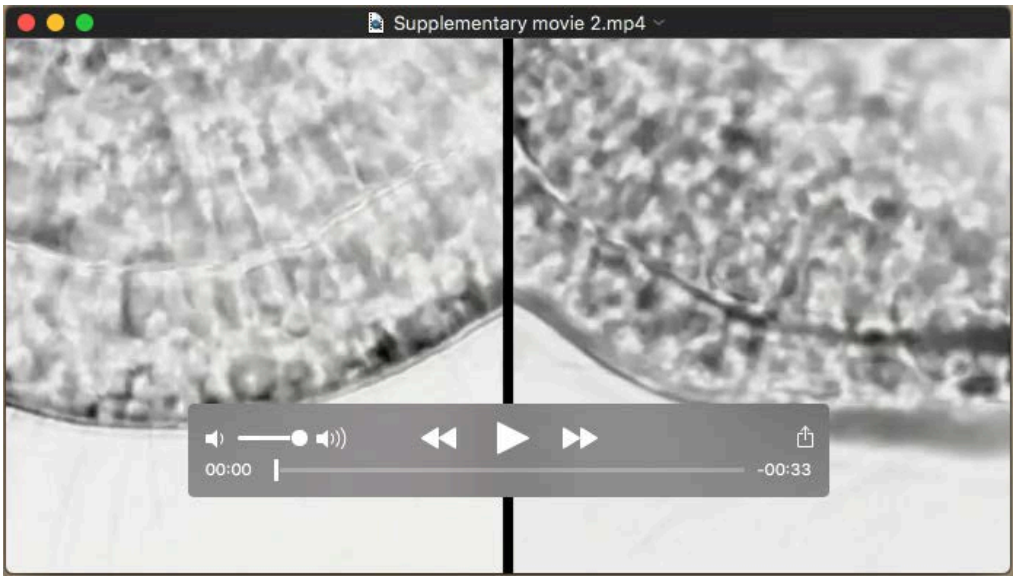

Movie 2. Ciliary motility is inhibited by 2% methylcellulose. Real-time movie of ciliary motility in control and methylcellulose treated embryo. A, B or C in the movie showed ciliary motility in epithelial ectoderm, neural ectoderm or gastrocoel roof plate, respectively. D in the movie showed neurula rotation. Motility of cilia on the epithelial ectodermal cells, neural ectodermal cells or gastrocoel roof plate cells was effectively inhibited by methylcellulose. Furthermore, neurula rotation was completely inhibited by methylcellulose.

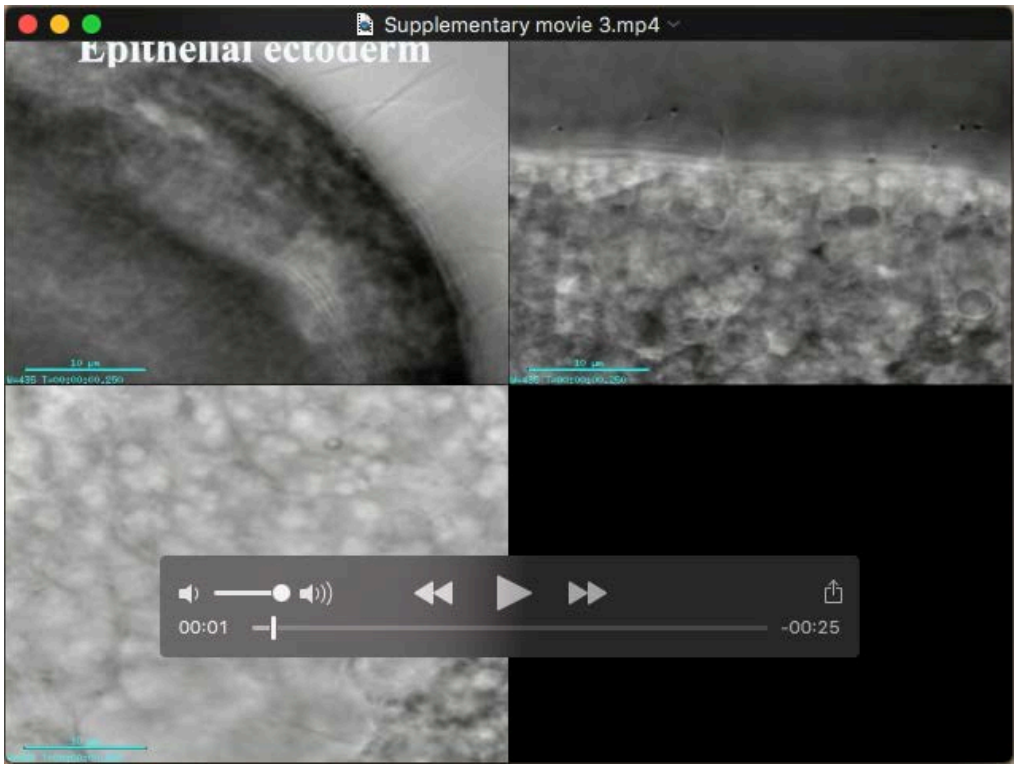

Movie 3. Cilia in early neurula embryos of amphioxus are motile, but do not rotate. Time-lapse movie of dorsal explant of early neurula (ventral view) revealed fast beating of long cilia on left-lateral epithelial ectodermal cells, and very low-frequency of beating of long cilia on gastrocoel roof plate cells, and medium-frequency beating of short cilia on anterior neural ectodermal cells. For better observation, the movie was slowed down to half of its original speed. The bars in the movie are 10 μm.